Bioactive Materials 6 (2021) 4707–4716

Contents lists available at ScienceDirect

Bioactive Materials

journal homepage: www.sciencedirect.com/journal/bioactive-materials

Platinum-crosslinking polymeric nanoparticle for synergetic chemoradiotherapy of nasopharyngeal carcinoma

Yuxun Ding [a,b], Xiaohui Xiao [a], Lingli Zeng [a], Qiuping Shang [a], Wei Jiang [a], Sha Xiong [a], Xiaohui Duan [a], Jun Shen [a], Ruibing Wang [c], Jinshan Guo [d], Yue Pan [a,*]

[a] Guangdong Provincial Key Laboratory of Malignant Tumor Epigenetics and Gene Regulation, Guangdong-Hong Kong Joint Laboratory for RNA Medicine, Department of Radiology, Medical Research Center, Sun Yat-Sen Memorial Hospital, Sun Yat-Sen University, Guangzhou, 510120, China
[b] Longgang E.N.T. Hospital & Shenzhen Key Laboratory of E.N.T., Institute of E.N.T., Shenzhen, Guangdong, 518116, China
[c] State Key Laboratory of Quality Research in Chinese Medicine, Institute of Chinese Medical Sciences, University of Macau, Macau SAR, China
[d] Department of Histology and Embryology, School of Basic Medical Sciences, Southern Medical University, Guangzhou, 510515, China

ARTICLE INFO

Keywords:
Nasopharyngeal carcinoma (NPC)
Chemoradiotherapy
Polymeric nanoparticles
Precise treatment

ABSTRACT

Despite extensive use of radiotherapy in nasopharyngeal carcinoma (NPC) treatment because of its high radiosensitivity, there have been huge challenges in further improving therapeutic effect, meanwhile obviously reducing radiation damage. To this end, synergistic chemoradiotherapy has emerged as a potential strategy for highly effective NPC therapy. Here, we developed RGD-targeted platinum-based nanoparticles (RGD-PtNPs, denoted as RPNs) to achieve targeted chemoradiotherapy for NPC. Such nanoparticles consist of an RGD-conjugated shell and a *cis*-platinum (CDDP) crosslinking core. Taking advantage of RGD, the RPNs may effectively accumulate in tumor, penetrate into tumor tissues and be taken by cancer cells, giving rise to a high delivery efficiency of CDDP. When they are fully enriched in tumor sites, the CDDP loaded RPNs can act as radiotherapy sensitizer and chemotherapy agents. By means of X-ray-promoted tumor cell uptake of nanoparticle and CDDP-induced cell cycle arrest in radiation-sensitive G2/M phases, RPNs may offer remarkable therapeutic outcome in the synergistic chemoradiotherapy for NPC.

1. Introduction

Nasopharyngeal carcinoma (NPC) is the most common cancer that originated from the nasopharynx, characterized by distinct geographical distribution and particularly prevalent in East and Southeast Asia [1–3]. Because NPC is highly sensitive to ionizing radiation, radiotherapy (RT) therefore has emerged as the primary and only curative treatment for non-metastatic NPC [1,4]. Unfortunately, the clinical radiotherapy may inevitably produce undesirable complications for head and neck cancer after treatment at this stage [5,6], because of the specific location of tumor, which is closely surrounded by and in close proximity to radiation dose-limiting organs such as the brain stem and spinal cord [2,7]. In undergoing radiotherapy, healthy cells in proximal tissues may also be damaged by high-dose X-ray or other types of radioactive ray, thus would cause many severe radiation-induced toxicities, such as temporal lobe neuropathy, late xerostomia, and trismus [8]. Moreover, despite the significant improvements in radiotherapy technique, radioresistances often occurred in many solid tumors during RT, leading to poor RT outcomes and negative prognosis [9–11].

To overcome the limitation of RT, chemotherapy is usually employed to combine with it in the synergistic treatment, via increasing the amount of DNA damage, inhibiting repair of nonlethal DNA damage, or cell cycle arrest into radiosensitive phases [10,12]. Taking advantage of the synergy of chemotherapy drug, chemoradiotherapy may significantly inhibit tumor growth, helping to ease radiotherapy-induced damages by reducing radiation dose. Meanwhile, such combined therapy may also relieve the side effects resulting from chemotherapy by minimizing the dose of medication. Actually, many studies have reported the results of chemotherapy combined with radiotherapy for the management of locoregional advanced cases of nasopharyngeal carcinoma in the past two decades [4,7,13]. Combination regimens varied between studies, but for the most part, *cis*-platinum (CDDP) was the chemoradiotherapy of choice, not only because of its strong chemotherapeutic efficacy but also for its considerable radiotherapy

Peer review under responsibility of KeAi Communications Co., Ltd.
* Corresponding author.
E-mail address: panyue@mail.sysu.edu.cn (Y. Pan).

https://doi.org/10.1016/j.bioactmat.2021.05.010
Received 2 December 2020; Received in revised form 28 April 2021; Accepted 8 May 2021
Available online 23 May 2021

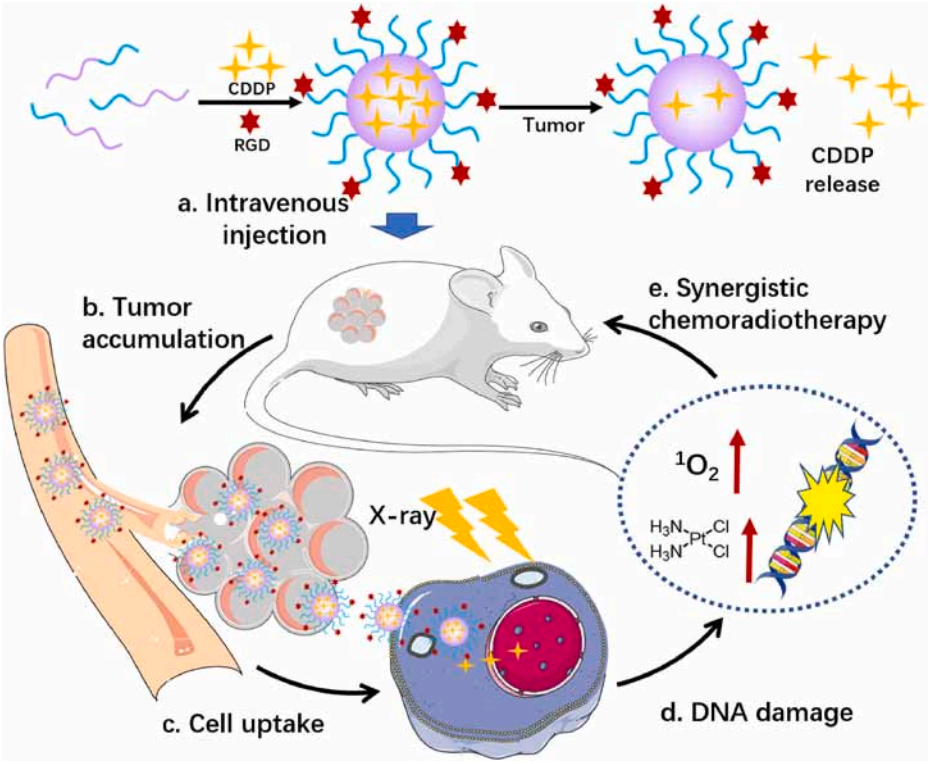

Scheme 1. Schematic illustration of the preparation and the application of RPNs in synergistic chemoradiotherapy.

sensitization performance [14,15].

With the development of nanotechnology, the strategy of platinum-based chemoradiotherapy can be well realized in the treatment of cancer [16–18]. In comparison with small-molecule chemoradiotherapy agents, the platinum-containing nanomedicines, such as the cisplatin-based nanoparticles (CDDP-NPs), display a good biodistribution and tumor-targeting capability *in vivo*, to a great extent, can reduce the biotoxicity of chemoradiotherapy agents and improve the therapeutic effect [19–21]. Especially, the emergence of polyamino acid nanomedicines shows admirable biocompatibility *in vivo* [22]. Nevertheless, huge challenges still existed in the therapy of NPC, resulting from the inferior tumor targeting ability of CDDP-NPs. In addition, the successful chemoradiotherapy of NPC heavily depends on the delivery efficiency. To this end, various targeted ligands, such as RGD peptide and folic acid (FA), have been applied to improve the targeted effect of nanomedicines [23]. Evidences suggested that the RGD receptors overexpress in many cancer cells and RGD-conjugated nano-carriers could target tumors efficiently [22]. Except for the enhanced permeability and retention (EPR) effect [24], the RGD-conjugated nanoparticles can effectively accumulate in tumor tissues through binding to the RGD receptor. Meanwhile, the RGD can also function as a tumor-penetrating peptide to improve the tumor penetration of nanoparticles [25,26], and thus achieved an efficient drug delivery.

Herein, we developed RGD-targeted platinum-based nanoparticles (RPNs) that display radiotherapy sensitization and chemotherapy performance for targeted chemoradiotherapy in the treatment of NPC (Scheme 1). The RPNs consist of an RGD-conjugated PEGlated shell and CDDP-crosslinked core. Taking advantage of the targeting performance of RGD and the EPR effect of nanoparticles in tumor sites, the RPNs can accumulate in cancer tissues, then efficiently bind to the RGD receptor distributed in the tumor cell membrane and be subsequently taken by cancer cells, giving rise to a high delivery efficiency of CDDP in tumor [22,24]. Upon internalizing into cancer cells, the CDDP loaded at RPNs can be acted as a chemotherapy agent and radiotherapy sensitizer to achieve double damage for the DNA of cancer cells. Importantly, the RPNs can arrest cell cycles into radiation-sensitive phases such as G2/M phases. Meanwhile, X-ray can increase the cellular uptake of CDDP. This unique feature of RPNs would significantly improve the therapeutic effect, and may also offer an alternative strategy to minimize the pain for the patient of NPC in the future.

2. Experimental section

2.1. Materials

NH_2-PEG_{5k}-b-PGlu was obtained from Guangzhou tansh-tech Ltd., China. *Cis*-platinum (CDDP) was acquired from J&K Chemical Ltd., USA. RGD (cyclo(-RGDfC) was purchased from Shanghai GL Biochem Ltd., China. Cy5-NHS ester was obtained from Shanghai YareBio Ltd., China.

2.2. Preparation of the RGD-targeted platinum-based nanoparticles (RPNs)

The platinum-based nanoparticles (PtNPs) were assembled in a PBS solution, driven by the coordination between CDDP and carboxyl group. Briefly, the NH_2-PEG-b-PGlu (50 mg) was dissolved in 20 mL PBS (pH 8.5, adjusted using NaOH solution), and was then added to a 20 mL CDDP solution (1 mg/mL) that treated with two equivalents of $AgNO_3$ solution. The mixture was stirred overnight in the dark at 60 °C. AgCl was removed by centrifugation at 5000 rpm for 15 min. The residual free CDDP and excess $AgNO_3$ were removed by dialysis in a PBS solution for 2 days. The RGD was conjugated to the PEG of PtNPs by amidation reaction and click reaction. In brief, the 3-Maleimidopropionic acid (0.43 mg, 0.5 e.q.) was reactivated by DCC (0.6 e.q.) and NHS (0.6 e.q.) in anhydrous tetrahydrofuran (THF) at room temperature for 24 h, and was then conjugated to the PEG of PtNPs by amidation reaction. Then, the RGD (0.2 e.q.) was added, followed by reaction at room temperature for 24 h to construct RPNs by click reaction chemistry of sulfhydryl and maleic anhydride. The RPNs solution was transferred into a dialysis bag (MWCO 5000) and dialyzed in PBS solution for 3 days.

2.3. Characterization of RPNs

The physicochemical properties of RPNs were determined using dynamic light scattering (DLS), zeta potential, and transmission electron microscopy (TEM). In this study, the RPNs solution was diluted to 0.1 mg/mL. The DLS measurements and zeta potential analysis were performed on Malvern granulometer. TEM samples were prepared by dropping the RPNs solution (0.05 mg/mL) onto a carbon-coated copper grid and dried slowly at desiccator, followed by observation with TEM. The loading rate of CDDP was determined using Inductively Coupled Plasma Mass Spectrometry (ICP-MS). For the structural characterization of RGD, the nanoparticles were obtained by lyophilization, followed by ^{1}H NMR in D_2O.

2.4. Stability assessment

The stability of RPNs was assessed in PBS and FBS solution, using DLS and Zeta potential. Briefly, 0.5 mL 0.2 mg/mL RPNs solution was added into 0.5 mL PBS solution and 0.5 mL 20% FBS solution, respectively. Then, the particles size and intensity of RPNs were observed at setting time points using DLS (0, 1, 2, 4, 8, 12, 24, and 48 h). With a similar method, the stability of RPNs was further assessed in 100% FBS by observing the intensity.

2.5. In vitro CDDP release

To simulate the environment of blood and tumor, the *in vitro* CDDP release of RPNs was performed in PBS (pH 7.4) and GSH solution (pH 6.5). Briefly, 1 mL of RPNs solution was added into a dialysis bag (MWCO 5000) and immersed in 9 ml of PBS or GSH solution. At fixed time intervals (0, 1, 2, 4, 6, 8, 12, 24, and 48 h), 1 mL of the solution outside the dialysis bag was taken out for ICP-MS analysis and replaced with an equal volume of fresh PBS or GSH solution.

2.6. Cell culture

The nasopharyngeal carcinoma cells (CNE-1) were cultured in RPMI-1640 medium, containing 5% (v/v) fetal bovine serum (FBS) and 1% (v/v) penicillin-streptomycin, in a cell incubator at 37 °C with 5% CO_2. When the cells reached 70% confluence, they were digested with 0.25% trypsin-EDTA, and subcultured in fresh RPMI-1640 medium.

2.7. Cytotoxicity assay

The cytotoxicity of RPNs was evaluated in 3T3 cells using CCK-8 kits. CDDP was employed as a controlled group. Briefly, 3T3 cells were seeded on 96-well plates at a density of 0.5×10^4 cells per well in 100 μL RPMI-1640 medium containing 10% FBS. After an incubation of 24 h, the CDDP and RPNs solutions (0, 0.1, 0.2, 0.5, 1, 2, 5, 10, 20, 50 μg CDDP/mL), were added to each well. After another 24 h' incubation, the culture medium was removed and replaced with a 10% CCK-8 solution. The cells were incubated in a humidified atmosphere at 37 °C with 5% CO_2 for 2 h, and were then determined by a microplate reader at 450 nm.

2.8. In vitro synergetic chemoradiotherapy

The *in vitro* synergetic effect of RPNs was performed in CNE-1 cells, using CCK-8 assay. In brief, CNE-1 cells were seeded into 96-well plates at a density of 0.5×10^4 cells per well in 100 μL RPMI-1640 medium contained 10% FBS, followed by an incubation of 24 h. The RPNs solutions with different CDDP concentrations (0, 0.1, 0.2, 0.5, 1, 2, 5, 10, 20, 50 μg/mL) were added to each well for 24 h incubation. Then the cells were treated with X-ray (0, 2, 4 Gy). 12 h later, the cells were treated with CCK-8 and determined by a microplate reader at 450 nm.

2.9. Clone formation assay

CNE-1 cells were seeded into 12-well plates at a density of 0.2×10^4 cells per well. After an incubation of 24 h, PBS (group 1) and RPNs (10 μg/mL, group 2 and 3) were added, followed by incubation for 1 day. Group 3 was then irradiated with an X-ray (2 Gy). Then, all groups were incubated in a humidified atmosphere at 37 °C with 5% CO_2. 1 day and 5 days later (denoted as Day 1 and Day 5), the clone formation in all groups were determined by optical microscope after staining using crystal violet.

2.10. Cell uptake

CNE-1 cells were seeded on 12-well plates at a density of 2×10^5 cells per well. After an incubation of 24 h, PBS (group 1) and Cy5-labeled RPNs (group 2 and 3, 0.1 mg/mL) were added, followed by 6-h incubation at 37 °C with 5% CO_2. Group 3 was treated with an X-ray (2Gy) and continued to incubate for 24 h. Treated cells were collected and determined using flow cytometry. To study the function of RGD in RPNs, non-RGD nanoparticles (PtNPs) were employed as the control group. CNE-1 cells were seeded on a confocal dish at a density of 2×10^4 cells per well for 24-h incubation, further incubated with FITC labeled RPNs and PtNPs, followed by observation using a confocal laser scanning microscope (CLSM).

2.11. Cell cycle analysis

CNE-1 cells were seeded on 12-well plates at a density of 2×10^4 cells per well. After an incubation of 24 h, the cells were treated with PBS (group 1), RPNs (group 2, 5 μg CDDP/mL), and RPNs (group 3, 10 μg CDDP/mL), followed by an incubation of 24 h. The cells were collected and fixed with 70% cooled ethanol for 2 h at 4 °C. After the treatment with RNase for 15 min at 37 °C, 50 μg/mL propidium iodide (PI) was added to the cells, followed by incubation for 15 min in the dark. Finally, the cells were treated with cell cycle kits and then determined using flow cytometry.

2.12. DNA damage detection

The CNE-1 cells were seeded onto 12-well plates and treated with PBS (group 1) and RPNs (group 2, 10 μg/mL) and RPNs+X-ray (group 2, 10 μg/mL, 2 Gy). The treated cells were stained with DAPI and FITC-labeled γ-H2AX antibody, followed by observation using CLSM.

2.13. CT imaging of RPNs

The RPNs solution was diluted to different concentrations (0, 0.1, 0.5, 0.75, 1, 2, 4, 6 mg Pt/mL) using PBS solution, followed by determination using a CT scanner. The CT signals were obtained from the associated CT imaging system. Then, the tumor-bearing mice were intravenously treated with RPNs (0.4 and 10 mg/mL, 100 μL), followed by observed using PET/CT scanner (Inveon) 1 h later.

2.14. The in vivo pharmacokinetics or biodistribution and tumor penetration

The *in vivo* pharmacokinetic study was conducted in BALB/c mice. Briefly, the mice (n = 3) were injected intravenously via the tail vein with Cy5-labeled RPNs and PtNPs at a dose of 5 mg/kg, respectively. At predetermined time points, blood samples (10 μL) were collected into heparin sodium solution (40 μL), followed by centrifugation at 4000 rpm for collecting plasma fractions, and then measured *via* multifunctional flow cytometry. Biodistribution and tumor penetration were performed in CNE-1-bearing BALB/c nude mice. Briefly, the mice (n = 3) were injected intravenously via the tail vein with Cy5-labeled RPNs and PtNPs at a dose of 5 mg/kg 24 h later, the mice were sacrificed for harvesting

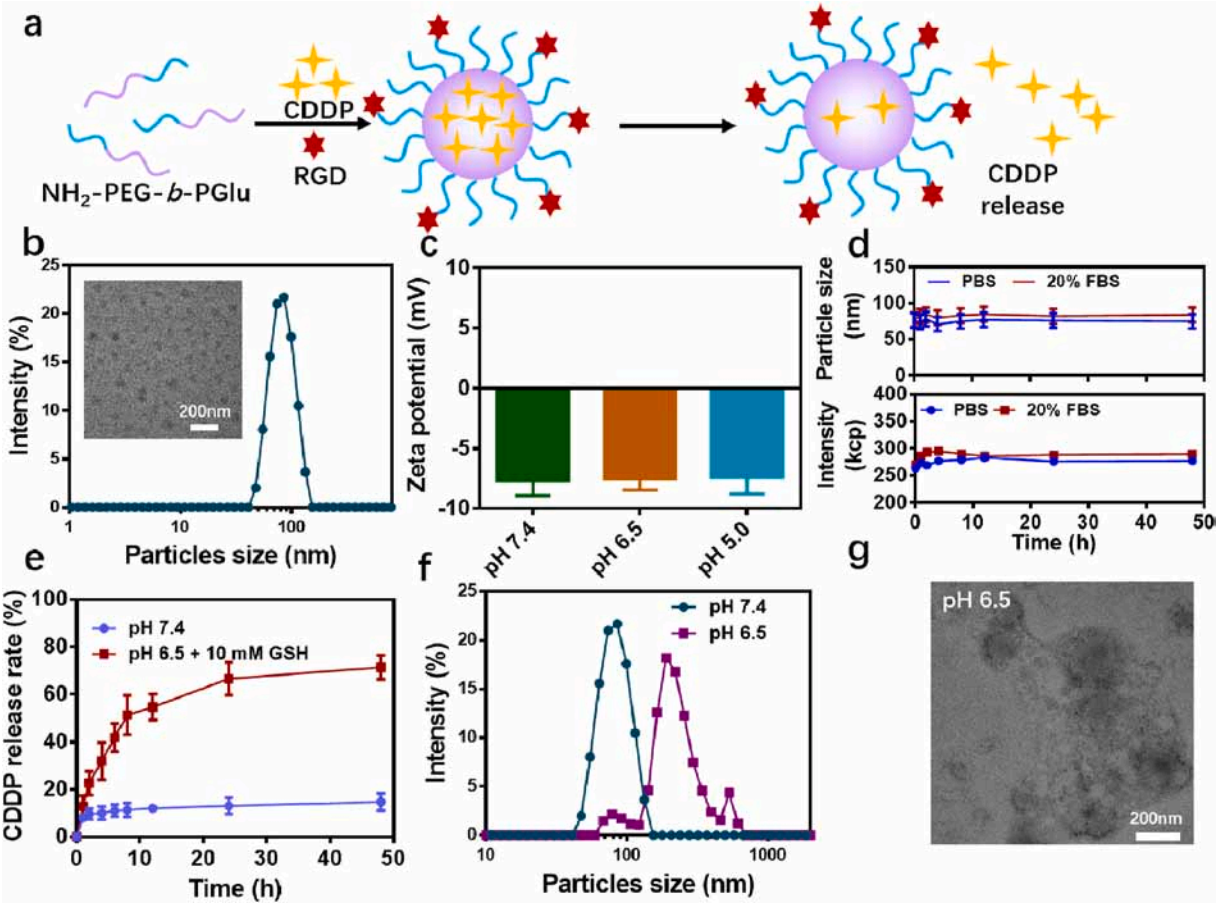

Fig. 1. Fabrication and characterization of RPNs. a. The preparation scheme of RPNs and the responsive release of CDDP from RPNs. b. The hydrodynamic diameters and TEM image of RPNs. c. Zeta potentials of RPNs. d. The stability of RPNs determined by particle size and intensity of RPNs over 48 hours. e. The *in vitro* pH-responsive CDDP release of RPNs. f. The particles size of RPNs in acidic condition at 48 h. g. The TEM image of RPNs in acidic condition at 48 h.

the major organs (heart, liver, spleen, lung, and kidney) and tumor. *Ex vivo* imaging was conducted by the Kodak IS *in vivo* FX imaging system. The tumor were collected, dehydrated by 30% sugar solution for 2 days, fixed with 4% formaldehyde solution for 2 days, and cut into 8 mm thick sections, followed by staining with DAPI and FITC-anti-CD31, and observation via CLSM.

2.15. The in vivo synergetic chemoradiotherapy of RPNs

The *in vivo* synergetic chemoradiotherapy of RPNs for NPC was determined in CNE-1 tumor-bearing nude mice. Male BALB/c nude mice aged 4–5 weeks were purchased from Guangdong Experimental Animal Center (Guangdong, China). All animal studies were approved by the Animal Care and Use Committee of the Sun Yat-sen University. Tumors were transplanted in BALB/c nude mice *via* a hypodermic injection of 1 $\times$ 10^6 CNE-1 cells suspended in 100 μL PBS/matrigel (1:1) solution in each mouse. The tumors volume was calculated length $\times$ width^2/2. When the tumor grew to 50 mm^3, tumor-bearing mice were randomly divided into six groups, and treated with PBS (group 1), PBS+X-ray (group 2), CDDP (group 3), CDDP+X-ray (group 4), RPNs (group 5), RPNs+X-ray (group 6). Respectively, the mice were treated with PBS, CDDP, and RPNs *via* tail vein injection at Day 0, Day 3 and Day 6, and administrated with X-ray at Day 1, Day 4 and Day 7. The dose of CDDP was fixed at 2 mg/kg, and the dose of X-ray was set at 2 Gy (Day 1), 2 Gy (Day 4), and 4 Gy (Day 7). Mice were monitored for tumor growth and weight loss at setting time points for three weeks. Finally, the mice were sacrificed by cervical dislocation under anesthesia.

2.16. Hematoxylin/eosin (H&E) and immunohistochemical staining

The tumors and the major organs of the treated mice in antitumor experiment were collected and immersed in 4% paraformaldehyde for 48-h fixation, followed by paraffin embedding. Then, the 12 μm-thick paraffin section in each tissue were prepared using a rotary microtome, and were then stained by hematoxylin/eosin (H&E). The resulting sections were observed via an optical microscope.

2.17. The qualification of DNA damage marker

Freezing sections were also obtained from the tumor of each group in the antitumor experiment, and were then stained using 4′,6-diamidino-2-phenylindole (DAPI, blue fluorescence) and FITC-labeled γ-H2AX antibody (green fluorescence), followed by systematic observation using a CLSM.

2.18. Statistical analysis

The IC50 was obtained from the statistical analysis using GraphPad Prism. The mean fluorescence intensity was analyzed using FlowJo VX. Immunofluorescence analysis was analyzed using Image J. Statistical analysis was operated by one-way ANOVA for multiple groups and Student's t-test for two groups. $P < 0.05$ was considered significant.

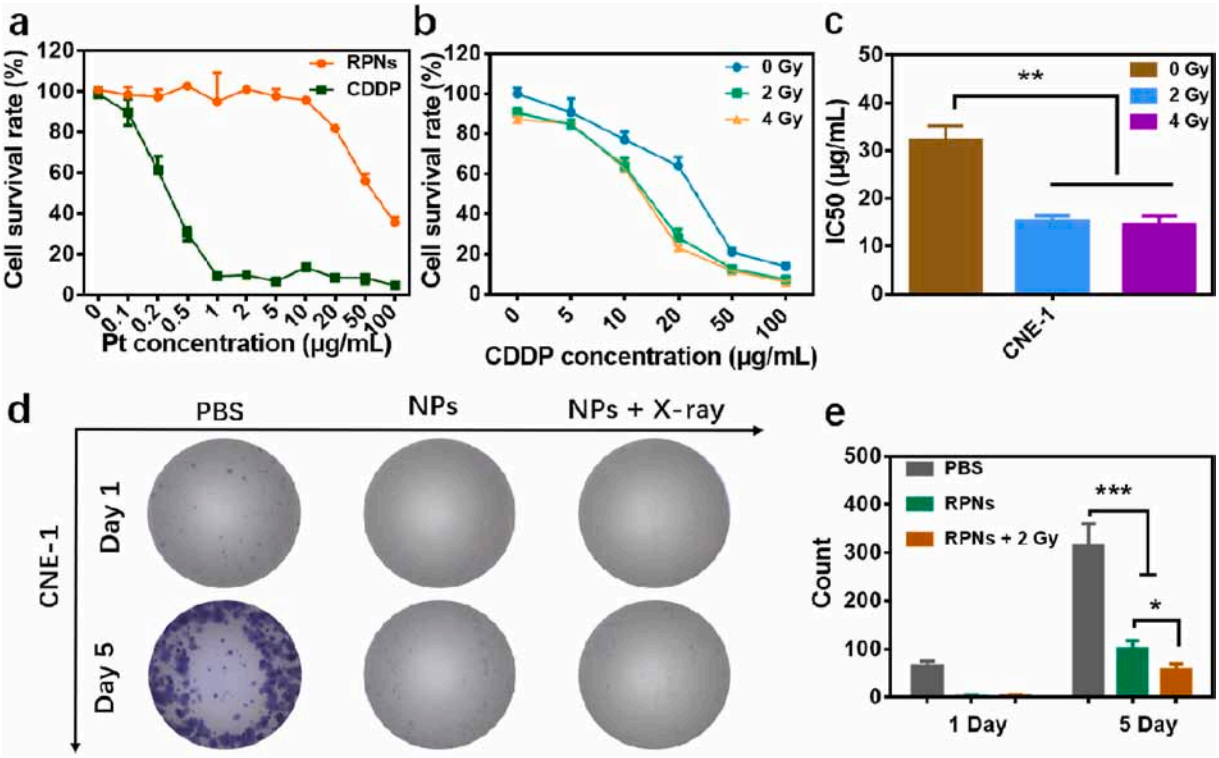

Fig. 2. *In vitro* synergistic therapeutic effect of RPNs. a. The cytotoxicities of CDDP and RPNs monitored in 3T3 cells. b-c. The cytotoxicities (b) and IC50 (c) for CNE-1 cells treated with RPNs and X-ray (0, 2, and 4 Gy). d-e. The clone formation (d) and statistical analysis (e) in CNE-1 cells after treating with PBS, RPNs, and RPNs+X-ray (2 Gy). Statistical analysis was operated by one-way ANOVA for multiple groups and Student's t-test for two groups. $^{*}P < 0.05$, $^{**}P < 0.01$, $^{***}P < 0.001$.

3. Results

3.1. Fabrication and characterization of RPNs

The preparation of RPNs was achieved via a two-step process. As illustrated in Fig. 1a, the platinum-based nanoparticles were synthesized through the self-assembly strategy, driven by the cross-linking of CDDP and carboxyl in NH_2-PEG-*b*-PGlu [27]. The loading efficiency of CDDP was determined to around 14.7% *via* ICP-MS. Then, an RGD peptide was employed as a model targeting ligand and conjugated to the end of PEG using amidation and click reaction. The successful formation of the polyplex was then confirmed by dynamic light scattering (DLS), transmission electron microscope (TEM) and zeta potentials. The results indicated that the average hydrodynamic diameters of RPNs were measured to be around 80 nm, with narrow size distribution and a well-defined spherical shape (Fig. 1b and c). In the 1H NMR spectra (Fig. S2), the appearance of the characteristic peak of benzene (7.0–7.5 ppm), attributed to RGD (cyclo(-RGDfC)), suggested the successful conjugation of RGD. The characteristic peak area ratio between the benzene in RGD and the PEG (2.5–3.0 ppm) in PEG-b-PGlu was determined to be around 1: 147, suggested that the RGD/PEG rate in RPNs was around 6.2%. RPNs consist of PEG shell and corss-linking core, thus we can estimate that the RGD modified degrees in RPNs are around 6.2%. Zeta potential analyses suggested that RPNs were negatively charged at different pH condition (pH 7.4, 6.5, and 5.0). With such uniform morphology, crosslinked core, negative surface and PEGlated shell, RPNs were expected to display excellent stability when functioning as a high-efficacy drug delivery system in cancer therapy. To demonstrate this assumption, the stability of RPNs were monitored by DLS and zeta potential over 48 h. In both PBS and FBS solution, negligible changes were observed in the particle size and intensity (Fig. 1e). Even in a complex environment that presented large amounts of protein (100% FBS, Fig. S3), RPNs can also exhibit outstanding stability.

3.2. Characterization of the tumor-microenvironment response of RPNs

In comparison with healthy tissues, the tumor shows a significantly low-pH, high-GSH, and hypoxia microenvironment, providing a point of penetration for targeted cancer treatment [19,20,28–30]. In this work, RPNs were precisely constructed by the crosslinking of CDDP and carboxyl, which show a remarkable response in the tumor environment. Therefore, we expected that RPNs can selectively release CDDP in the tumor microenvironment instead of normal organs. To investigate the responsive performance of RPNs, we used PB solution (pH 7.4) and GSH solution (PBS, pH 6.5, 10 mM) to simulate the bloodstream and tumor microenvironment for studying the CDDP release. As shown in Figs. 1e and S4a, the cumulative release of CDDP was less than 20% in 48 h, revealing a low CDDP release under the physiological condition (pH 7.4). While at low-pH and high-GSH tumor microenvironment, the cumulative release was remarkably increased to more than 60% in 24 h, resulting from the rupture of CDDP-crosslinking core, suggesting noteworthy sensibility for tumor microenvironment. Furthermore, the GSH concentration dependence of CDDP release again confirmed that RPNs showed a good response to the tumor microenvironment (Fig. S4b). To further investigate the responsive performance of RPNs, we observed the particle size and the structure of RPNs using DLS and TEM. As shown in Fig. 1f, due to the disassembly of RPNs, noticeable swelling and dissociation were observed in DLS and TEM. The DLS result indicated that the particle size of RPNs increased up to 200 nm after 48-h incubation at pH 6.5 (Fig. 1f). Also, the swollen and separate RPNs displayed in the TEM image again confirmed the noteworthy sensibility in tumor environment (Fig. 1g). These results implied that RPNs showed great potential to selectively release CDDP in tumor site, possibly giving rise to a high-efficient treatment for NPC, and potentially reducing the damage to healthy tissues at the same time.

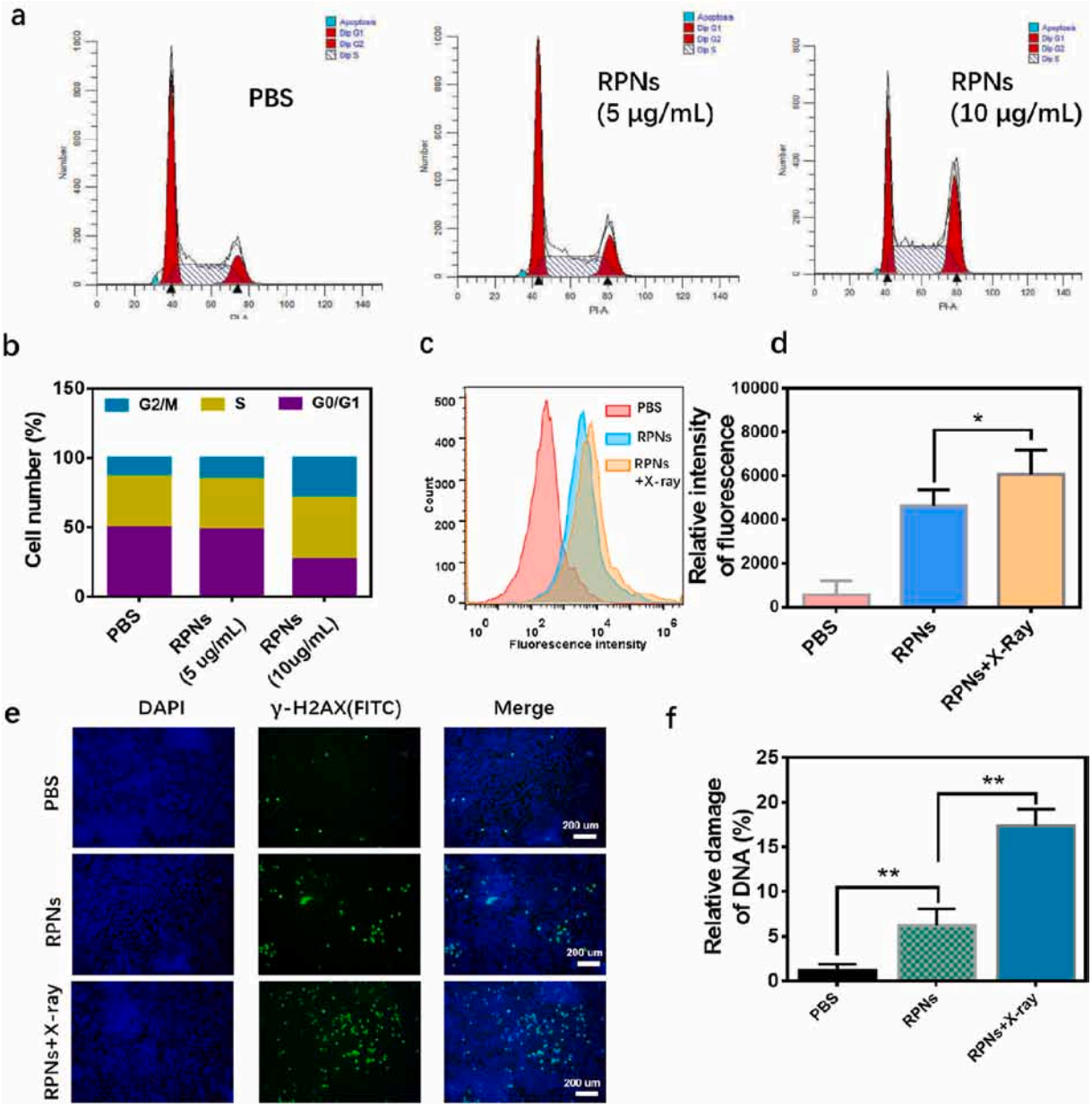

Fig. 3. *In vitro* synergistic mechanism of RPNs for CNE-1 cells. a. Flow cytometric analysis of cell cycles for CNE-1 cells, which treated with PBS, RPNs (5 μg/mL), and RPNs (10 μg/mL). b. Quantitative analysis of the G1, G2/M, S phases of CNE-1 cells treated with PBS, RPNs (5 μg/mL), and RPNs (10 μg/mL)). c-d. Flow cytometric (c) and quantitative analysis (d) of cell uptake in CNE-1 cells treated with PBS, Cy5-RPNs, and Cy5-RPNs+X-ray. e-f. γ-H2AX immunofluorescent staining (e) and statistical analysis (f) in CNE-1 cells, administrated with PBS, RPNs, and RPNs+X-ray. Statistical analysis was operated by Student's t-test for two groups. $^{*}P < 0.05$, $^{**}P < 0.01$, $^{***}P < 0.001$.

3.3. Synergistic treatment of RPNs in vitro

Accordingly, the RPNs may display a considerable synergistic property of chemoradiotherapy for the cancer cells of NPC, because of the heavily loaded CDDP. Here, the cytotoxicity of RPNs was firstly performed in the 3T3 cells. As shown in Fig. 2a, the cell survival rates treated with RPNs were higher than that of CDDP at a different dosage. Further analysis also revealed that the IC50 of RPNs was more than 50 μg Pt/mL for healthy cells, while that of CDDP was less than 0.5 μg Pt/mL. Those results confirmed that RPNs can reduce the toxicity of CDDP by more than ten times, and thus may relieve side effects in the treatment. Then, the *in vivo* synergistic effect of RPNs for NPC was performed in the human nasopharyngeal carcinoma cells (CNE-1). As Fig. 2b, the cell survival rates that treated with RPNs and X-ray (2 and 4 Gy) can be noticeably decreased compared with that of only managed with RPNs, suggesting that the X-ray can further improve the killing activity of RPNs for CNE-1 cells. Also, the dramatical depressed IC50 observed in the X-ray-treatment groups further revealed the sensitization effect of X-ray for the chemotherapy of CDDP (Fig. 2c). Next, we evaluated the synergistic effect by cloning formation experiments. Within 5 days, extremely low cell proliferation was observed in the RPNs + X-ray group, while apparent proliferations were showed in the other groups (RPNs and PBS groups) (Figs. 2d and S5). Further significance analysis also uncovered the most prominent inhibitory effect in RPNs + X-ray group (Fig. 2e), which suggested that the RPNs can show the best inhibition for cancer cells when cooperating with X-ray.

Inspired by the good synergy in CNE-1 cells, we attempted to further explore their collaborative mechanisms. Recently, several reports suggested that CDDP can arrest cell cycles into radiation-sensitive phases such as G2/M phases [31], thus can further enhance radiation-induced

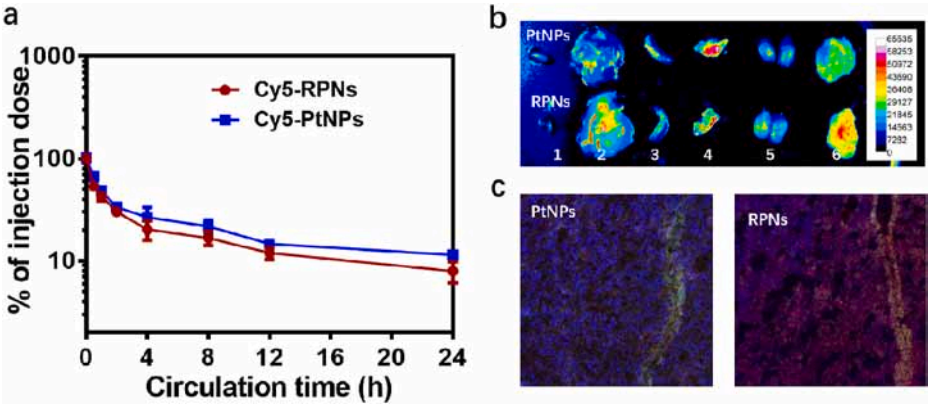

Fig. 4. The *in vivo* delivery efficiency of RPNs. The *in vivo* pharmacokinetics (a), biodistribution (b) (1. Heart, 2. Liver, 3. Spleen, 4. Lung, 5. Kidney, 6. Tumor) and tumor penetration (c) of RPNs and PtNPs.

cell damage [10]. Also, evidences suggested that X-ray exposure could promote cell uptake and slow down cell efflux of nanoparticles, likely providing a feasible way to improve the chemotherapeutic efficacy of nanomedicines [32]. To explore the collaborative mechanisms, we analyzed the cell cycle and the cell uptake in CNE-1 cells after treating with RPNs and X-ray, using a cell flow technique. As shown in Fig. 3a and b, the cell cycles of CNE-1 cells in G2/M phase were arrest from 13.35% to 15.43% and 28.77% when they were administrated with RPNs (5 μg/mL and 10 μg/mL, respectively), revealing a considerable sensibilization for the radiotherapy in CNE-1 cells. Meanwhile, an enhanced fluorescence signal (Cy5) was observed in CNE-1 cells after treating with Cy5-labeled RPNs (Cy5-RPNs) and X-ray (2 Gy), compared to that of only treated Cy5-RPNs. This result indicated that X-ray can increase the cellular uptake of RPNs, potentially achieving intensive chemotherapy of CDDP for NPC. Because of the potentials in simultaneous sensibilization for radiotherapy and chemotherapy, the RPNs was expected to achieve a synergistic destroy for the DNA in cancer cells, when they were combined with X-ray. To confirm our hypothesis, the γ-H2AX, a major DNA damage marker, was detected to assess the therapeutic effect of chemoradiotherapy. After systematical treatment, the CNE-1 cells were stained with FITC-labeledγ-H2AX antibody and observed using CLSM. In the CLSM images, the strongest green fluorescent signal appeared on the RPNs + X-ray group, and a moderate-intensity fluorescent signal was showed in the RPNs group, while few fluorescent signals can be found when they were treated with PBS solution (Fig. 3e). The further statistical analysis of CLSM images was also performed in Fig. 3f, confirming the satisfactory *in vitro* chemoradiotherapy-collaboration effect of RPNs for CNE-1 cells.

3.4. CT imaging potentials of RPNs

The minimization of side effects is a primary task and superiority for nanomedicines in cancer therapy. Except for the optimization design of nanomedicines, an image-guided technology, especially in simultaneous imaging, highly needed in chemoradiotherapy to guide an accurate treatment [10,17]. By and large, an image-guided strategy can further reduce accidental injury for healthy tissues. Actually, the RPNs may show a satisfactory CT imaging performance attributed to the high-loaded CDDP. To prove this hypothesis, we observed the CT images of RPNs with different concentration via a CT scanner. As the concentration of Pt increases, the CT signal displayed a significant enhancement (Fig. S7), suggesting that RPNs may act as a contrast agent for CT imaging. To further study the potential application of RPNs in image-guided therapy, we investigated the CT imaging capability in tumor-bearing mice. As shown in Fig. S8, a strong CT signal was observed in the tumor site after treatment with high-dose NPs (10 mg/mL, 100 μL). However, a much weaker CT signal was acquired after low-dose treatment of RPNs, indicating that a better CT imaging performance improvement remains a major challenge for RPNs-based image-guided therapy.

3.5. The in vitro and in vivo delivery efficiency of RPNs

RGD is one widely used tumor targeted ligand to improve cellular uptake, tumor accumulation and penetration in cancer therapy. To investigate the function of RGD for tumor target, we studied the cell uptake of FITC-labeled RPNs (FITC-RPNs) and FITC-labeled PtNPs (FITC-PtNPs) in CNE-1 cells using CLSM. A stronger green fluorescent signal was observed in the cells treated with FITC-RPNs, compared with that of the FITC-PtNPs-treated group (Fig. S6), suggesting that RGD can effectively improve the targeted effect of nanomedicines for CNE-1 cells. To investigate the *in vivo* delivery efficiency of RPNs, the pharmacokinetics were first evaluated in BALB/c mice. According to the results, there were around 10% RPNs and PtNPs in the blood at 24 h (Fig. 4a), suggesting an excellent circulation performance *in vivo*. In the tumor of *ex vivo* images, a stronger fluorescent signal was observed in the group treated with Cy5-RPNs, while a weaker fluorescence was observed in the Cy5-PtNPs-treated group (Fig. 4b), indicating a satisfactory tumor accumulation of RPNs *in vivo*. In the CLSM images, a stronger red fluorescence and deeper distribution were found in the Cy5-RPNs-treated group (Fig. 4c), suggesting the better tumor penetration of RPNs, in comparison with PtNPs. Taken together, the RPNs showed an excellent pharmacokinetics pharmacokinetic profile, superior tumor accumulation and penetration, thereby achieving effective delivery of CDDP for NPC therapy.

3.6. In vivo synergistic chemoradiotherapy of RPNs

Encouraged by the satisfactory synergistic effect *in vitro*, RPNs has a very high probability of achieving effective cancer treatment for NPC. Thus, we assessed their synergistic therapeutic effect in the NPC-xenograft tumor nude mice. For better comparison, PBS and CDDP were selected as controlled groups. When the tumor grows to 50 mm^3, the tumor-bearing mice were randomly divided into six groups and the antitumor efficacy was evaluated by the systemic administration of PBS, PBS+X-ray, CDDP, CDDP+X-ray, RPNs, and RPNs+X-ray, followed by monitoring the tumor volumes and body weights of the animals. A dose of 2 mg CDDP/kg body weight and X-ray (2 Gy) was administered to each mouse three times every 3 days (RPNs treated at Day 0, Day 3 and Day 6, X-ray treated at Day 1, Day 4 and Day 7) (Fig. 5a). As shown in Fig. 5b, all mice treated with the CDDP formulations showed certain degrees of inhibition in the tumor growth over 21 days, compared with PBS groups (PBS and PBS+X-ray). However, the tumor inhibition effect of CDDP can be significantly improved when they are loading in a

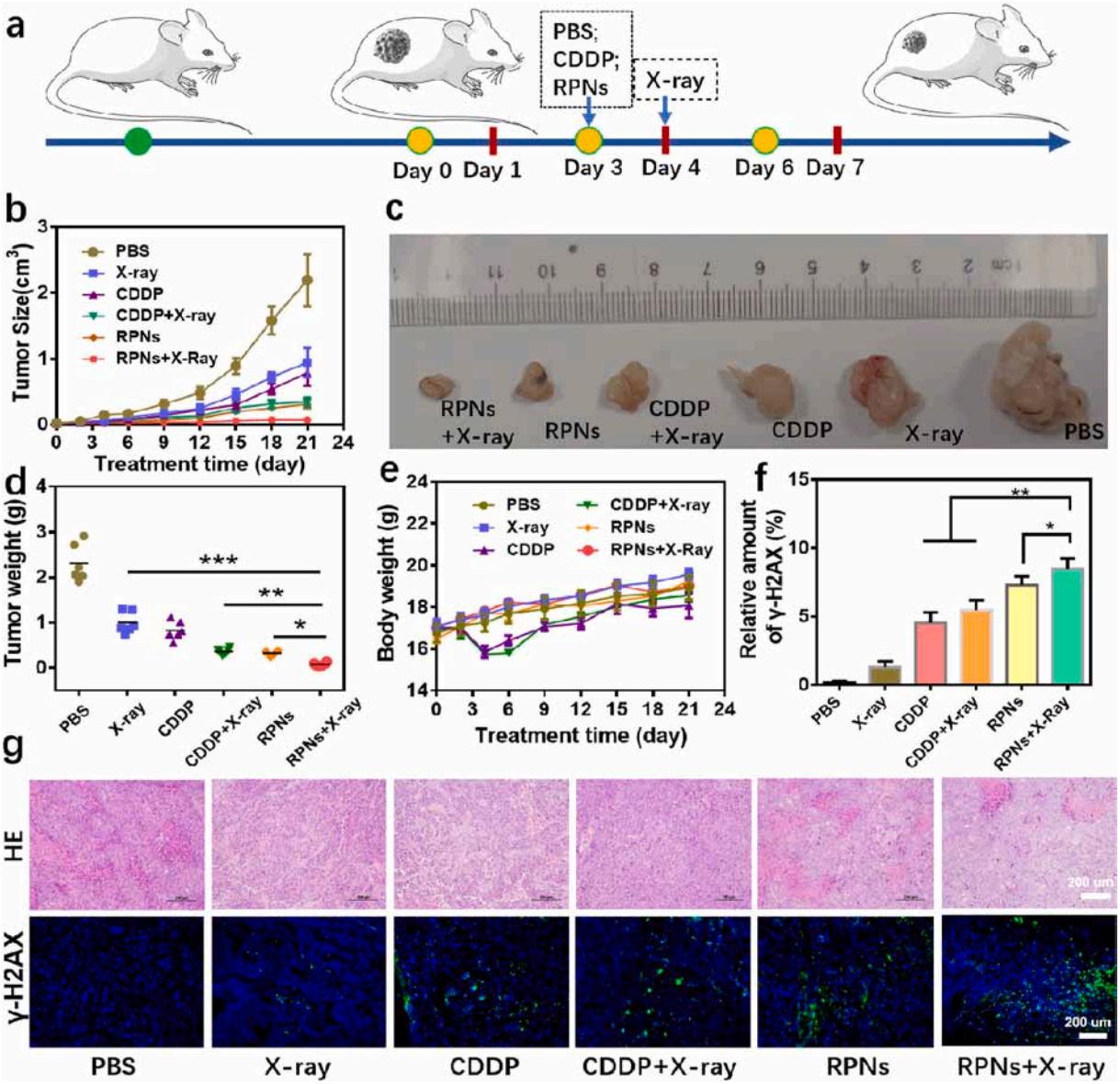

Fig. 5. *In vivo* radiochemotherapy studies. a. Schematic illustration of the treatment for NPC-bearing nude mice. b-f. Tumor volume (b), photographs (c), weight (d), body weight (e), DNA damage levels (f) of mice with various treatments including PBS, X-ray, CDDP, CDDP+X-ray, RPNs, and RPNs+X-ray at the dose of 2 Gy and 2 mg CDDP/kg. g. The effect of radiochemotherapy on the histopathology and γ-H2AX immunofluorescent staining from mice in each group over 21 days. Data represent the mean ± SD (n = 6). Statistical analysis was operated by one-way ANOVA for multiple groups and Student's t-test for two groups. *P < 0.05, **P < 0.01, ***P < 0.001.

tumor-targeted nanoparticle, because the tumor-targeted nanoparticles can improve the accumulation of CDDP in tumor sites. More importantly, the best growth inhibition for NPC was observed in the RPNs+X-ray group, attributed to the enchantments of X-ray, indicating the significant *in vivo* synergistic therapeutic effect in our chemoradiotherapy treatment. To further evaluate the synergistic effects, H&E staining and γ-H2AX immunofluorescent staining examinations were conducted for the evaluation of cell apoptosis and DNA damage in each group. The highest level of tumor apoptosis after simultaneous administration of RPNs and X-ray were showed in Fig. 5g, revealing the highest antitumor efficacy of RPNs+X-ray among all formulations. Also, the strongest fluorescence signal was observed in the RPNs+X-ray group (Fig. 5f and g), again confirming the best tumor suppression for NPC when combined RPNs with X-ray.

Finally, the undesirable biodistribution of CDDP may lead to the relief in the side effects caused by the nonspecific toxicity of CDDP for healthy tissues, which is one of the major concerns for the application of nanomedicines. In this system, the CDDP was loaded in a polymeric nanoparticle, with good biocompatibility and well biocompatibility, to a greater extent, can reduce the undesirable adverse reaction. This conclusion was confirmed by monitoring the body weights of the mice over the treatments. The body weights of the mice treated with RPNs and RPNs+X-ray changed slightly during the treatment, whereas significant weight loss was observed from the mice treated with free CDDP (CDDP and CDDP+X-ray), as shown in Fig. 5e. Moreover, the histologic sections of main organs (heart, liver, spleen, lung, and kidney) in RPNs+X-ray treated mice on the 21st day exhibited no obvious histopathological abnormalities. Those results revealed no apparent toxicities caused by RPNs *in vivo*, suggesting that RPNs may be a safe agent for *in vivo* application in NPC therapy.

4. Discussions

Radiotherapy and platinum-based chemotherapy are the primary

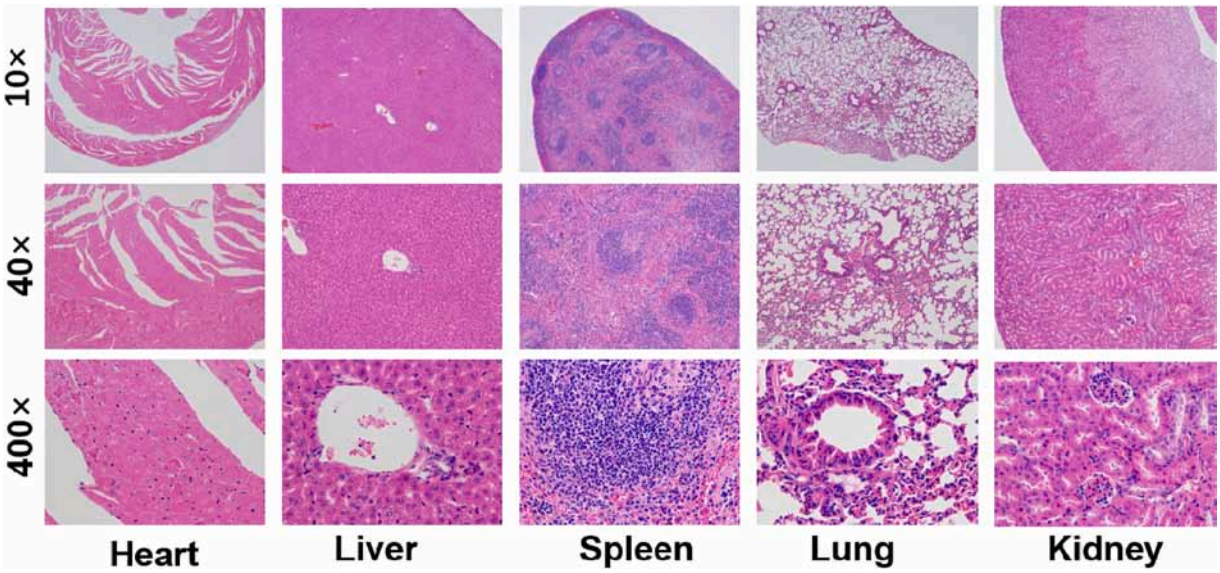

Fig. 6. *In vivo* biocompatibility and biodegradability of RPNs. H&E staining of major organs (heart, liver, spleen, lung, and kidney) from NPC-bearing mice treated with RPNs+X-ray on the 21st day.

treatment for non-metastatic NPC [1,4,7]. Radiotherapy combined with chemotherapy, to a certain extent, can improve the therapeutic effect for NPC, but usually suffer from severe radiation-induced damage as well as chemotherapy-induced toxicities because of the high therapeutic dose [8–10]. In this study, the CDDP, an agent combined with radiotherapy sensitization and chemotherapy, was loaded in a polyamino acid nanoparticle with excellent biocompatibility [22,33]. In the *in vitro* performance evaluation, such nanoparticles can steadily spread in the PBS solution, with an average size of around 80 nm and a well-defined spherical shape even in the presence of large amounts of protein (Fig. 1b–d). Compared to dissociative CDDP, the RPNs can reduce the toxicity of CDDP for healthy cells by more than ten times (Fig. 2a), by and large, may relieve the patient's pain in the treatment. In the blood circulation, such nanomedicines, with a particle size from 50 nm to 200 nm, may easily avoid renal elimination and endoplasmic reticulum clearance from the liver and spleen. Meanwhile, such nanoparticles can also accumulate and penetrate tumor tissues, with the help of RGD and the EPR effect in solid tumor [20,22,24]. Importantly, the CDDP was quickly released from RPNs in the acidic tumor microenvironment (Fig. 1e) to react the chemotherapy performance, implying that RPNs show a great potential to selectively induce the tumor cell apoptosis *in vivo*.

In previous studies, shreds of evidence suggested that CDDP-based nanoparticles can also act as a radiotherapy sensitizer [15,16]. Here, we have confirmed that RPNs can significantly induce cell apoptosis (Fig. 2b and c) and inhibit cell proliferation (Fig. 2d and e) for CNE-1 cells when combined with X-ray. This synergistic effect may attribute to the arrest effect for the cell cycle of CDDP and the promotion in cell uptake of X-ray [2,10,32]. Using a cell flow technique, we have successfully confirmed that RPNs can arrest cell cycles of CNE-1 cells into radiation-sensitive G2/M phases (Fig. 3a and b), and the X-ray can also increase the cell uptake of RPNs (Fig. 3c and d). Therefore, such nanoparticles can effectively destroy the DNA in the cancer cells (Fig. 3e and f), potentially giving rise to high-efficiency chemoradiotherapy for NPC. With the help of RGD, the RPNs can easily accumulate in tumor (Fig. 4b) and disfuse deeply in tumor tissues (Fig. 4c), and taken by cancer cells (Fig. S6), giving rise to an effective delivery of CDDP for NPC therapy.

Encouraged with the well-design structure, *in vitro* treatment effect, *in vivo* delivery effect and the *in vivo* antitumor activity were also evaluated in CNE-1-bearing nude mice. The results suggested that RPNs can effectively inhibit tumor growth by combining with radioactive rays (Fig. 5), and showed good biocompatibility *in vivo* (Fig. 6), implied that RPNs may provide a safe nanomedicine for the chemoradiotherapy of NPC in the future.

5. Conclusion

In summary, we have demonstrated an RGD-targeted platinum-based nanoparticle for the chemoradiotherapy of NPC. Such NPs are capable of targeting the over-expressed RGD receptor in the tumor cell membrane, thus can achieve efficient killer for cancer cells by enhancing the cell uptake of CDDP. When entering the living body, the RPNs is able to accumulate into the tumor through the EPR effect and the targeted function of RGD, enhancing the content of CDDP in tumor sites and improving the biodistribution of CDDP *in vivo*, thus maximized the synergistic efficiency of chemoradiotherapy and minimize the side effect caused by CDDP, offering a high-efficiency nanomedicine for the chemoradiotherapy of NPC in the future.

CRediT authorship contribution statement

Yuxun Ding: Conceptualization, Methodology, Investigation, Writing – original draft. **Xiaohui Xiao:** Data curation, Investigation. **Lingli Zeng:** Writing – review & editing. **Qiuping Shang:** Data curation. **Wei Jiang:** Visualization. **Sha Xiong:** Visualization. **Xiaohui Duan:** Data curation. **Jun Shen:** Writing – review & editing. **Ruibing Wang:** Writing – review & editing. **Jinshan Guo:** Writing – review & editing. **Yue Pan:** Conceptualization, Supervision, Writing – review & editing.

Declaration of competing interest

The authors declare no competing interests.

Acknowledgements

We acknowledge the financial support from Guangdong Basic and Applied Basic Research Foundation for Distinguished Young Scholars (2020B1515020027), the grant from Guangzhou Science and Technology Bureau (202002020070, 202102010181, 202102010007), the Fundamental Research Funds for the Central Universities (19ykpy108, 20ykpy93), Guangdong Science and Technology Department (2020B1212060018, 2020B1212030004), Shenzhen Key Medical

Discipline Construction Fund (SZXK039), the Guangdong Basic and Applied Basic Research Fund Foundation (2019A1515110204, 2020A1515010523), the Yat-sen Scientific Research Project (YXQH202018), Shenzhen Innovation of Science and Technology Commission (LGKCYLWS2020089), the National Key R&D Program of China (2017YFE0102400), Shenzhen Science and Technology Program (JCYJ20190807160401657).

Appendix A. Supplementary data

Supplementary data to this article can be found online at https://doi.org/10.1016/j.bioactmat.2021.05.010.

References

[1] M.L.K. Chua, J.T.S. Wee, E.P. Hui, A.T.C. Chan, Lancet 387 (2016) 1012–1024.
[2] W.I. Wei, J.S.T. Sham, Lancet 365 (2005) 2041–2054.
[3] Y.-P. Chen, A.T.C. Chan, Q.-T. Le, P. Blanchard, Y. Sun, J. Ma, Lancet 394 (2019) 64–80.
[4] P. Blanchard, A. Lee, S. Marguet, J. Leclercq, W.T. Ng, J. Ma, A.T.C. Chan, P.-Y. Huang, E. Benhamou, G. Zhu, D.T.T. Chua, Y. Chen, H.-Q. Mai, D.L.W. Kwong, S. L. Cheah, J. Moon, Y. Tung, K.-H. Chi, G. Fountzilas, L. Zhang, E.P. Hui, T.-X. Lu, J. Bourhis, J.P. Pignon, Lancet Oncol. 16 (2015) 645–655.
[5] J.J. Caudell, J.F. Torres-Roca, R.J. Gillies, H. Enderling, S. Kim, A. Rishi, E. G. Moros, L.B. Harrison, Lancet Oncol. 18 (2017) e266–e273.
[6] J. Bourhis, J. Overgaard, H. Audry, K.K. Ang, M. Saunders, J. Bernier, J.-C. Horiot, A. Le Maître, T.F. Pajak, M.G. Poulsen, B. O'Sullivan, W. Dobrowsky, A. Hliniak, K. Skladowski, J.H. Hay, L.H.J. Pinto, C. Fallai, K.K. Fu, R. Sylvester, J.-P. Pignon, Lancet 368 (2006) 843–854.
[7] R. You, Y.-P. Liu, P.-Y. Huang, X. Zou, R. Sun, Y.-X. He, Y.-S. Wu, G.-P. Shen, H.-D. Zhang, C.-Y. Duan, S.H. Tan, J.-Y. Cao, J.-B. Li, Y.-L. Xie, Y.-N. Zhang, Z.-Q. Wang, Q. Yang, M. Lin, R. Jiang, M.-X. Zhang, Y.-J. Hua, L.-Q. Tang, A.-H. Zhuang, Q.-Y. Chen, L. Guo, H.-Y. Mo, Y. Chen, H.-Q. Mai, L. Ling, Q. Liu, M.L. K. Chua, M.-Y. Chen, Jama Oncol. 6 (2020) 1345–1352.
[8] B. Zhang, Z. Mo, W. Du, Y. Wang, L. Liu, Y. Wei, Oral Oncol. 51 (2015) 1041–1046.
[9] J.K. Tuan, T.C. Ha, W.S. Ong, T.R. Siow, I.W. Tham, S.P. Yap, T.W. Tan, E.T. Chua, K.W. Fong, J.T. Wee, Radiother. Oncol. 104 (2012) 305–311.
[10] G. Song, Y. Chao, Y. Chen, C. Liang, X. Yi, G. Yang, K. Yang, L. Cheng, Q. Zhang, Z. Liu, Adv. Funct. Mater. 26 (2016) 8243–8254.
[11] S. Shi, R. Vissapragada, J. Abi Jaoude, C. Huang, A. Mittal, E. Liu, J. Zhong, V. Kumar, Bioact. Mater. 5 (2020) 233–240.
[12] J. Ma, H.-Q. Mai, M.-H. Hong, H.-Q. Min, Z.-D. Mao, N.-J. Cui, T.-X. Lu, H.-Y. Mo, J. Clin. Oncol. 19 (2001) 1350–1357.
[13] R. You, Y.S. Cao, P.Y. Huang, L. Chen, Q. Yang, Y.P. Liu, X. Zou, Y.N. Zhang, R. Jiang, M.X. Zhang, C.Y. Duan, A.H. Lin, M.H. Hong, M.Y. Chen, Theranostics 7 (2017) 4825–4835.
[14] Y. Sun, W.-F. Li, N.-Y. Chen, N. Zhang, G.-Q. Hu, F.-Y. Xie, Y. Sun, X.-Z. Chen, J.-G. Li, X.-D. Zhu, C.-S. Hu, X.-Y. Xu, Y.-Y. Chen, W.-H. Hu, L. Guo, H.-Y. Mo, L. Chen, Y.-P. Mao, R. Sun, P. Ai, S.-B. Liang, G.-X. Long, B.-M. Zheng, X.-L. Feng, X.-C. Gong, L. Li, C.-Y. Shen, J.-Y. Xu, Y. Guo, Y.-M. Chen, F. Zhang, L. Lin, L.-L. Tang, M.-Z. Liu, J. Ma, Lancet Oncol. 17 (2016) 1509–1520.
[15] L. Zhang, Y. Huang, S. Hong, Y. Yang, G. Yu, J. Jia, P. Peng, X. Wu, Q. Lin, X. Xi, J. Peng, M. Xu, D. Chen, X. Lu, R. Wang, X. Cao, X. Chen, Z. Lin, J. Xiong, Q. Lin, C. Xie, Z. Li, J. Pan, J. Li, S. Wu, Y. Lian, Q. Yang, C. Zhao, Lancet 388 (2016) 1883–1892.
[16] M. Zhang, C.T.t. Hagan, Y. Min, H. Foley, X. Tian, F. Yang, Y. Mi, K.M. Au, Y. Medik, K. Roche, K. Wagner, Z. Rodgers, A.Z. Wang, Biomaterials 169 (2018) 1–10.
[17] Z. Wang, D. Shao, Z. Chang, M. Lu, Y. Wang, J. Yue, D. Yang, M. Li, Q. Xu, W. F. Dong, ACS Nano 11 (2017) 12732–12741.
[18] S. Liu, J. Pan, J. Liu, Y. Ma, F. Qiu, L. Mei, X. Zeng, G. Pan, Small 14 (2018) 1703968.
[19] Y. Ding, J. Liu, X. Li, L. Xu, C. Li, L. Ma, J. Liu, R. Ma, Y. An, F. Huang, Y. Liu, L. Shi, Mater. Chem. Front. 3 (2019) 1159–1167.
[20] Y.X. Ding, J.J. Liu, Y.M. Zhang, X. Li, H.L. Ou, T.J. Cheng, L. Ma, Y.L. An, J.F. Liu, F. Huang, Y. Liu, L.Q. Shi, Nanoscale Horiz. 4 (2019) 658–666.
[21] Y. Deng, E. Li, X. Cheng, J. Zhu, S. Lu, C. Ge, H. Gu, Y. Pan, Nanoscale 8 (2016) 3895–3899.
[22] T.J. Cheng, Y.M. Zhang, J.J. Liu, Y.X. Ding, H.L. Ou, F. Huang, Y.L. An, Y. Liu, J. F. Liu, L.Q. Shi, ACS Appl. Mater. Interfaces 10 (2018) 5296–5304.
[23] J. Wu, P. Ning, R. Gao, Q. Feng, Y. Shen, Y. Zhang, Y. Li, C. Xu, Y. Qin, G.R. Plaza, Q. Bai, X. Fan, Z. Li, Y. Han, M.S. Lesniak, H. Fan, Y. Cheng, Adv. Sci. 7 (2020) 1902933.
[24] Y. Ding, Y. Xu, W. Yang, P. Niu, X. Li, Y. Chen, Z. Li, Y. Liu, Y. An, Y. Liu, W. Shen, L. Shi, Nano Today 35 (2020).
[25] K. Wang, X.F. Zhang, Y. Liu, C. Liu, B.H. Jiang, Y.Y. Jiang, Biomaterials 35 (2014) 8735–8747.
[26] X.Y. Jiang, H.L. Xin, Q.Y. Ren, J.J. Gu, L.J. Zhu, F.Y. Du, C.L. Feng, Y.K. Xie, X. Y. Sha, X.L. Fang, Biomaterials 35 (2014) 518–529.
[27] C.N. Xu, Y.B. Wang, Z.P. Guo, J. Chen, L. Lin, J.Y. Wu, H.Y. Tian, X.S. Chen, J. Contr. Release 295 (2019) 153–163.
[28] X. Zeng, G. Liu, W. Tao, Y. Ma, X. Zhang, F. He, J. Pan, L. Mei, G. Pan, Adv. Funct. Mater. 27 (2017) 1605985.
[29] Z. Zhang, Q. Wang, Q. Liu, Y. Zheng, C. Zheng, K. Yi, Y. Zhao, Y. Gu, Y. Wang, C. Wang, X. Zhao, L. Shi, C. Kang, Y. Liu, Adv. Mater. 31 (2019), e1905751.
[30] C. Zheng, Q. Wang, Y. Wang, X. Zhao, K. Gao, Q. Liu, Y. Zhao, Z. Zhang, Y. Zheng, J. Cao, H. Chen, L. Shi, C. Kang, Y. Liu, Y. Lu, Adv. Mater. 31 (2019) e1902542.
[31] Z. Wei, X. Yin, Y. Cai, W. Xu, C. Song, Y. Wang, J. Zhang, A. Kang, Z. Wang, W. Han, Int. J. Nanomed. 13 (2018) 1505–1524.
[32] X. Yi, L. Chen, J. Chen, D. Maiti, Z. Chai, Z. Liu, K. Yang, Adv. Funct. Mater. (2018) 28.
[33] X. Li, X. Cai, Z. Zhang, Y. Ding, R. Ma, F. Huang, Y. Liu, J. Liu, L. Shi, Nano Lett. 20 (2020) 4454–4463.